Optical Materials 169 (2026) 117563

Contents lists available at ScienceDirect

Optical Materials

journal homepage: www.elsevier.com/locate/optmat

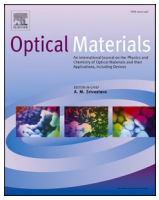

Research Article

# Upconversion photoluminescence in WSSe alloy monolayer under uniaxial tensile strain

Shrawan Roy [a], Jie Gao [b,*], Xiaodong Yang [a,**]

[a] Department of Mechanical and Aerospace Engineering, Missouri University of Science and Technology, Rolla, MO, 65409, USA
[b] Department of Mechanical Engineering, Stony Brook University, Stony Brook, NY, 11794, USA

ARTICLE INFO

*Keywords:*
WSSe alloy monolayer
Upconversion photoluminescence
Uniaxial tensile strain

ABSTRACT

The optical responses of monolayer transition metal dichalcogenides (1L-TMDs) can be tuned effectively by using mechanical strain. In this work, the tuning of upconversion photoluminescence (UPL) emission in 1L-WSSe alloy by applying uniaxial tensile strain is investigated. When the uniaxial tensile strain is changed from 0 % to 1.02 %, the peak position of UPL emission has a redshift of around 25.6 nm, and the UPL intensity goes up with an exponential function of the applied strain as the upconversion energy difference is varied from −197 meV to −131 meV. The sublinear power dependence for UPL emission in 1L-WSSe alloy indicates the multiphonon-mediated upconversion emission process involved with one photon. The demonstrated strain-tunable UPL emission in 1L-TMD alloys will advance potential applications in upconversion photonic devices and flexible optoelectronics.

## 1. Introduction

Monolayer transition metal dichalcogenides (1L-TMDs) including $WS_2$, $WSe_2$, $MoS_2$, and $MoSe_2$ are sub-nanometer thick direct-bandgap 2D semiconductor materials with intriguing optical and optoelectronic properties [1–4]. These properties can be further tailored with 1L-TMD alloys which are synthesized by mixing the different concentrations of either the transition metal atoms ($Mo_{(1-y)}W_ySe_2$ and $Mo_{(1-y)}W_yS_2$) [5–7] or the chalcogen atoms ($MoS_{2(1-x)}Se_{2x}$ and $WS_{2(1-x)}Se_{2x}$) [8–10]. In particular, 1L-$WS_{2(1-x)}Se_{2x}$ is a unique alloy possessing continuously tunable bandgap in a broad frequency range from 1.65 eV of 1L-$WSe_2$ to 2.0 eV of 1L-$WS_2$ at room temperature by varying the alloy chemical compositions. Upconversion photoluminescence (UPL) is an optical phenomenon with photon emission at a higher energy compared with the photon absorbed in the material. UPL emission processes have been extensively explored in various material systems including quantum-well heterostructures [11], colloidal quantum dots [12], rare-earth doped solids [13], dye molecules [14,15], lanthanide-doped upconversion nanoparticles [16], along with 1L-TMD flakes [17–25], providing many practical applications in different areas like displays [26], photovoltaics [27], bioimaging [28,29], lasing [30], as well as optical refrigeration [31]. The optical responses of TMDs including photoluminescence (PL), UPL, Raman scattering, optical reflection, and optical absorption can be dynamically tuned by strain engineering, which is a useful technique for varying the crystal lattice structure and the bandgap of TMDs [17–21,32–41]. Mechanical strain can be applied to TMDs by different approaches such as forming wrinkles [38,41], transferring to patterned substrates [39,40], and bending flexible substrates like polycarbonate (PC) [17–19,36,37]. Although the strain tuned optical responses of 1L-TMDs have been reported in several studies, the strain tuning of optical responses especially the UPL emission in 1L-TMD alloys remains unexplored. The strain tuning of UPL emission in 1L-TMDs and their alloys plays an important role in the development of future UPL-based flexible optoelectronic devices with promising functionalities such as dynamically tunable emission wavelength, enhanced intensity, and precise mechanical strain detection, which will enable many applications in bioimaging, energy harvesting, strain sensing, and quantum light emission. Distinguished from binary 1L-TMDs with the fixed optical bandgaps, the optical bandgaps of ternary 1L-TMD alloys can be continuously tuned in a broad frequency range depending upon the chalcogen concentration, which enables the tunable UPL emission properties in 1L-TMD alloys by varying the constituent element concentration. Furthermore, unlike binary 1L-TMDs, 1L-TMD alloys support multiple optical phonon modes due to

* Corresponding author.
** Corresponding author.
*E-mail addresses:* jie.gao.5@stonybrook.edu (J. Gao), yangxia@mst.edu (X. Yang).

https://doi.org/10.1016/j.optmat.2025.117563
Received 19 April 2025; Received in revised form 13 September 2025; Accepted 26 September 2025
Available online 26 September 2025

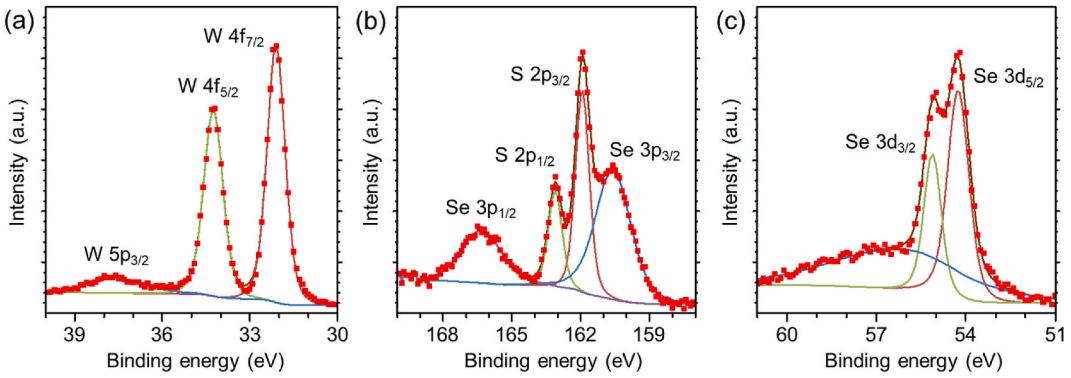


**Fig. 1.** High-resolution XPS spectra of (a) W 4f, (b) S 2p and Se 3p, (c) Se 3d for WSSe alloy.

chalcogen disorder and lattice distortion, leading to multiple pathways for phonon-assisted upconversion processes. The strain tuning in 1L-TMD alloys will further vary the optical bandgaps and UPL emission characteristics and affect the phonon-assisted upconversion channels, which will provide the opportunities for studying the unique UPL emission processes in the complex and tunable TMD alloy platforms that are different from binary TMDs.

Here, the UPL emission in 1L-WSSe alloy prepared from mechanical exfoliation under uniaxial tensile strain is demonstrated, as well as the strain tuned PL emission. A three-point bending apparatus is utilized for exerting uniaxial tensile strain on 1L-WSSe alloy which is transferred onto a flexible PC substrate. When the uniaxial tensile strain exerted on 1L-WSSe alloy varies from 0 % to 1.02 %, the peak position of UPL emission has a redshift of around 25.6 nm which corresponds to a gauge factor in strain tuning with a value of 65.1 meV/% strain, and the UPL intensity increases as an exponential function of the applied strain by 4.9 times under the excitation at 761 nm as the upconversion energy difference varies from −197 meV to −131 meV. The sublinear power dependence for UPL emission in 1L-WSSe alloy shows the multiphonon-mediated upconversion emission process involved with one photon. These results will provide new scopes for building future strain tunable and switchable upconversion photonic devices and flexible optoelectronics based on TMD alloys.

## 2. XPS analysis and 1L-WSSe alloy transferred on PC substrate

The X-ray photoelectron spectroscopy (XPS) measurements are performed on a mechanically exfoliated WSSe alloy flake from a bulk WSSe crystal ($x \approx 0.5$) grown by flux zone method (2D Semiconductors) to determine the chemical composition. Fig. 1(a)–(c) display the recorded high-resolution XPS spectra around the binding energy regions of W 4f, S 2p, Se 3p, and Se 3d with the corresponding fitted peaks. As depicted in Fig. 1(a), the feature peaks of W $4f_{7/2}$, W $4f_{5/2}$, and W $5p_{3/2}$ are obtained at the binding energies of 32.1, 34.3, and 37.6 eV, respectively. Fig. 1(b) presents both the S 2p doublet and the Se 3p doublet with the S $2p_{3/2}$, S $2p_{1/2}$ peaks at 161.9 and 163.1 eV and the Se $3p_{3/2}$, Se $3p_{1/2}$ peaks at 160.6 and 166.3 eV. The peaks corresponding to Se $3d_{5/2}$ and Se $3d_{3/2}$ are observed at 54.3 and 55.1 eV in Fig. 1(c). The binding energies of the elements are consistent with the $W^{4+}$, $S^{2-}$ and $Se^{2-}$ states, indicating the formation of $WS_{2(1-x)}Se_{2x}$ alloy. According to the compositional stoichiometry analysis from the XPS spectra, the quantitative composition ratio of Se/(S + Se) in $WS_{2(1-x)}Se_{2x}$ alloy is determined as $x = 0.48$, which is very close to the value of 0.5.

1L-WSSe alloy flakes are prepared through mechanical exfoliation from the bulk crystal using scotch tape. Multiple exfoliation steps are used to separate thin layers of WSSe with 1L samples from the bulk WSSe crystal. The tape containing multiple WSSe thin flakes is subsequently placed gently on the polydimethylsiloxane (PDMS) film atop a glass slide. After 1 h, the tape placed on the PDMS film is gently removed, leaving multilayer and monolayer WSSe alloy flakes on the PDMS surface. The 1L-WSSe alloy flakes left on the PDMS surface are identified by the contrast of microscopic image and the characteristic Raman spectra and PL spectra. The rectangular flexible substrate (15 mm by 65 mm) is prepared from a PC board with the thickness of 0.25 mm. The identified 1L-WSSe alloy flakes attached on the PDMS surface are then transferred at the central area of the rectangular PC substrate through the dry transfer technique [17,36,37,42], by utilizing a microscope system integrated with a micromanipulator to accurately align the monolayers with the substrate center. The reflection microscopic image of a 1L-WSSe alloy flake transferred on the PC substrate is presented in Fig. 2 (a), as indicated by the white arrow. Fig. 2(b) represents the schematic illustration of three-point bending apparatus to apply uniaxial strain onto 1L-WSSe alloy, where three rigid rods are used as the pivotal points in manipulating the deflection of the PC substrate so that the uniaxial tensile strain is exerted at the central region of the PC substrate. The uniaxial strain level exerted on the 1L-WSSe alloy flake at the substrate center can be calculated by $\varepsilon = 6Dt/L^2$, in which $L$ represents the distance in two opposing rods (25.4 mm), $t$ represents the thickness of rectangular PC substrate (0.25 mm), while $D$ represents the vertical displacement for the central rod [17,36].

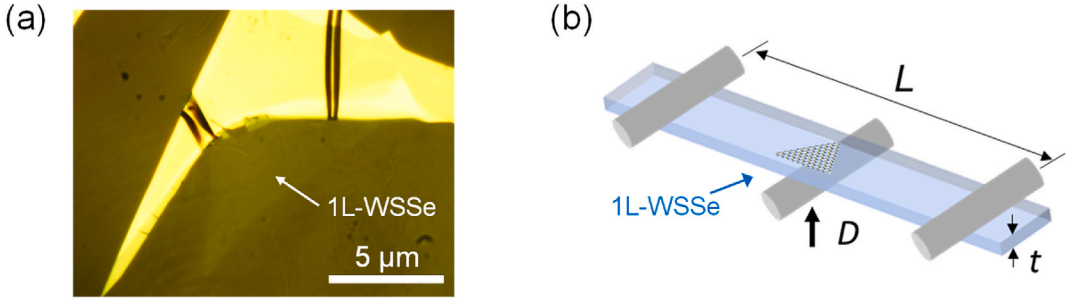


**Fig. 2.** (a) Reflection microscopic image of a 1L-WSSe alloy flake transferred on rectangular PC substrate, with 1L-WSSe region indicated by the white arrow. (b) Schematic illustration of three-point bending apparatus for exerting uniaxial strain onto 1L-WSSe alloy.

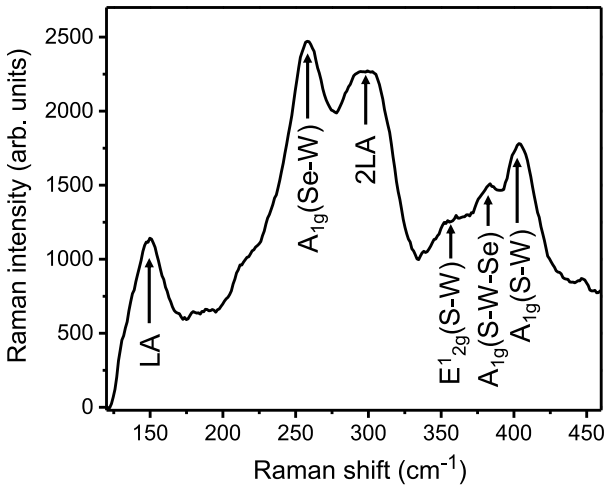


**Fig. 3.** Raman spectrum of 1L-WSSe alloy flake on rectangular PC substrate acquired using a 532 nm laser.

## 3. UPL emission in 1L-WSSe alloy under uniaxial strain

The Raman spectrum of 1L-WSSe alloy flake on rectangular PC substrate is acquired using a continuous-wave 532 nm laser by collecting the signal reflected from the 1L-WSSe alloy flake via one 50X long working distance objective lens with NA = 0.42 coupled to an optical spectrometer (Horiba, iHR 550) with one 532 nm longpass edge filter. Fig. 3 plots the measured Raman spectrum of 1L-WSSe alloy flake, which contains all six distinct characteristic phonon vibrational modes of 1L-WSSe alloy at room temperature. The Raman spectrum shows four optical phonon modes with the Raman shifts at 258 $cm^{-1}$ ($A_{1g}$ (Se–W)), 360 $cm^{-1}$ ($E^1_{2g}$ (S–W)), 384 $cm^{-1}$ ($A_{1g}$ (S–W–Se)), and 404 $cm^{-1}$ ($A_{1g}$ (S–W)), together with two additional peaks assigned to the longitudinal acoustic (LA) phonon mode with the Raman shift at 150 $cm^{-1}$ and its second-order replica (2LA) at 298 $cm^{-1}$. These featured Raman modes of 1L-WSSe alloy flake match with the previous Raman measurements for 1L-$WS_{2(1-x)}Se_{2x}$ alloys [9,10].

Fig. 4(a) and (b) show the measured uniaxial strain dependent PL spectra under the excitation at 532 nm and UPL spectra under the excitation at 761 nm with continuous-wave lasers at room temperature from 1L-WSSe alloy flake on flexible rectangular PC substrate. The same optical setup as the Raman measurement is used to characterize the PL and UPL spectra from 1L-WSSe alloy flake with the corresponding 532 nm longpass filter and two 750 nm shortpass filters, respectively. As shown in the black curve in Fig. 4(a), the PL spectrum at 0 % strain presents the PL peak position of 682 nm (1.82 eV) for the 1L-WSSe alloy flake, which is in agreement with the previous PL measurements of 1L-WSSe flakes [9,10]. It is known that the optical bandgap of ternary 1L-$WS_{2(1-x)}Se_{2x}$ alloy follows a linear relationship with the chalcogen concentration as $E_g(WS_{2(1-x)}Se_{2x}) = (1-x)E_g(WS_2) + xE_g(WSe_2)$, where $x$ is the Se/(S + Se) ratio. By considering the optical bandgap values of 2.0 eV for 1L-$WS_2$ and 1.65 eV for 1L-$WSe_2$, the estimated Se concentration

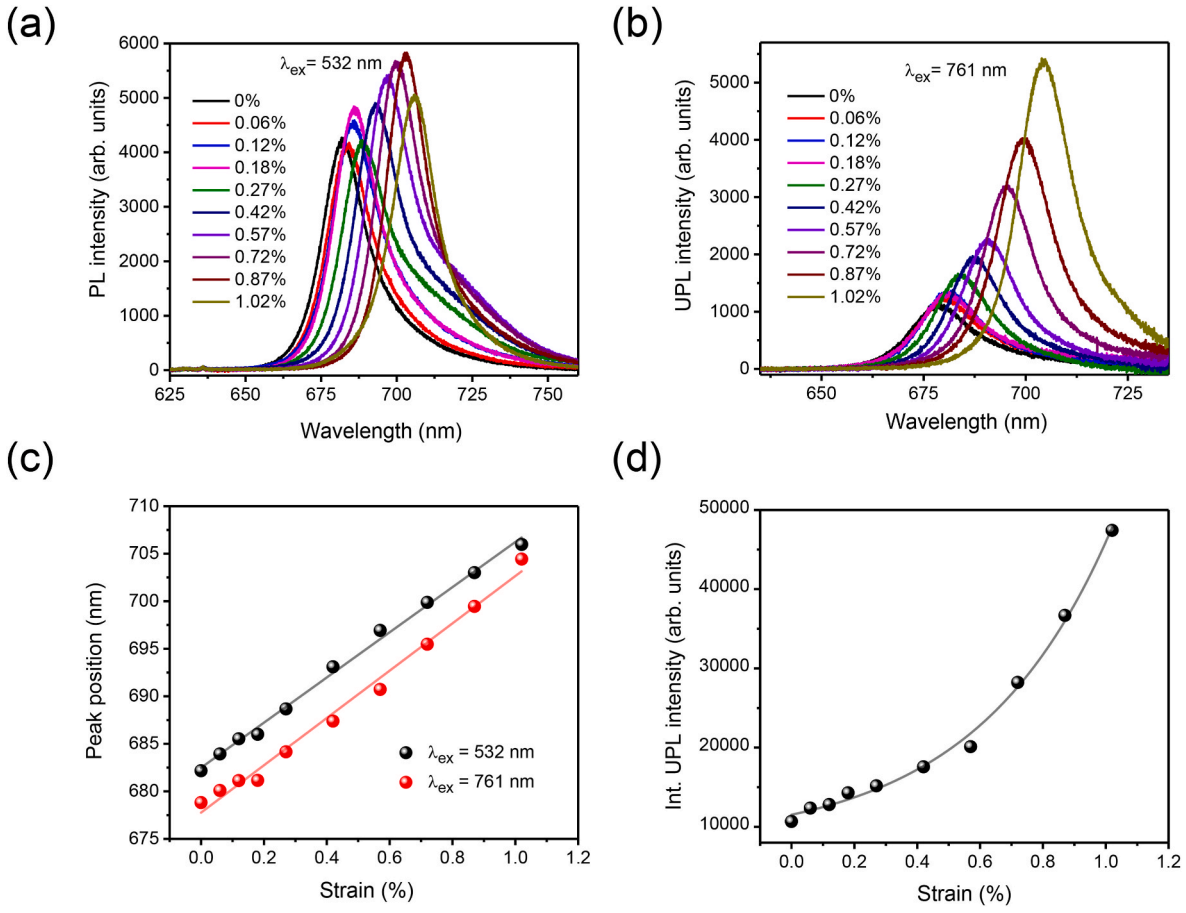


**Fig. 4.** (a) Strain dependent PL spectra from 1L-WSSe alloy excited at 532 nm with the exerted uniaxial tensile strain from 0 % to 1.02 %. (b) Strain dependent UPL spectra under the excitation at 761 nm. (c) PL and UPL peak positions depending on the applied uniaxial tensile strain. The black line and red line represent the linear fitting corresponding to each excitation wavelength. (d) Integrated UPL intensity depending on the uniaxial strain. The black curve represents the exponential fitting. (For interpretation of the references to colour in this figure legend, the reader is referred to the Web version of this article.)

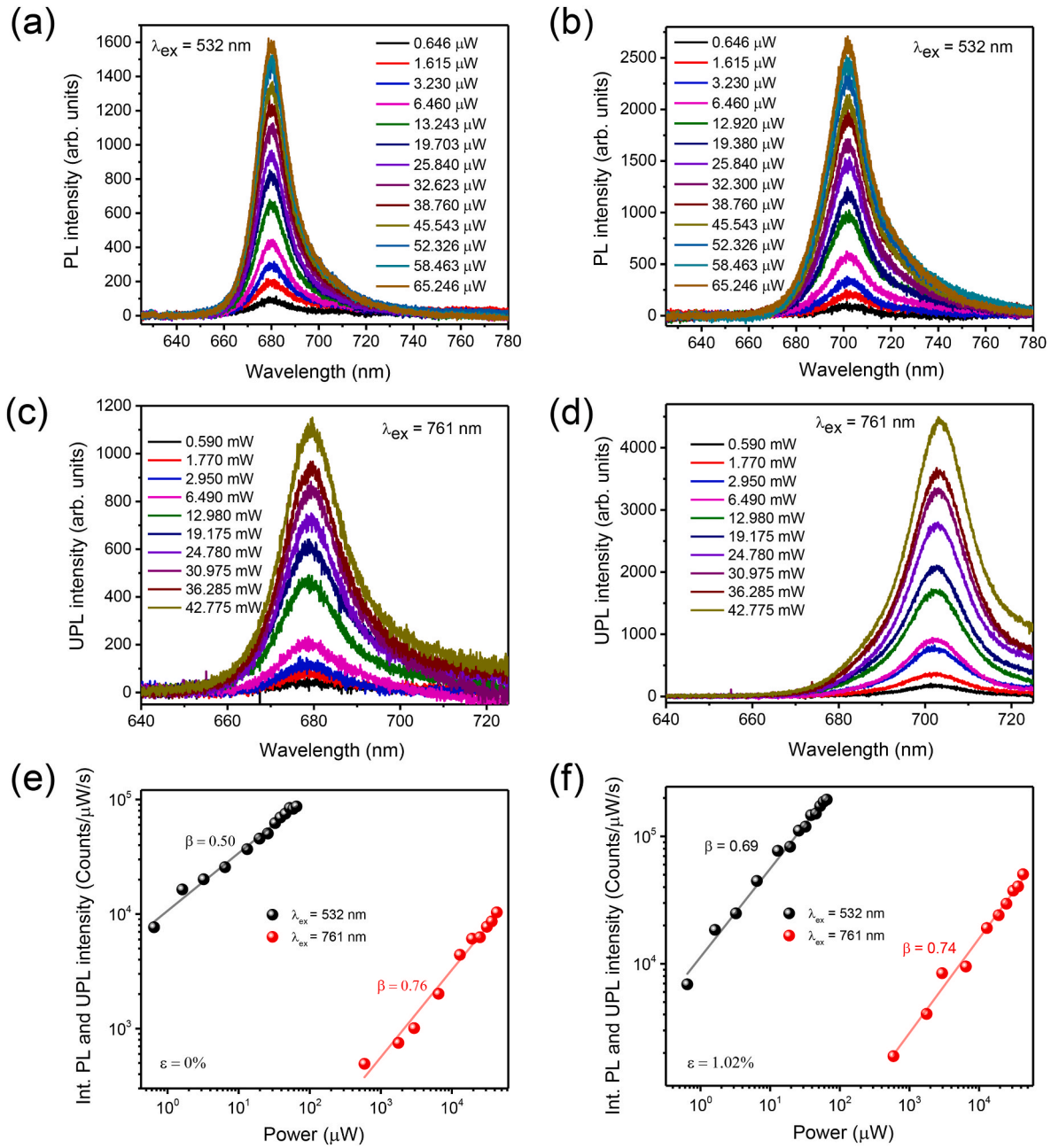


**Fig. 5.** Power dependence of PL and UPL spectra from 1L-WSSe alloy under 532 nm and 761 nm excitations with the applied uniaxial strains of (a),(c) 0 % and (b),(d) 1.02 %. (e),(f) Integrated PL intensity and UPL intensity depending on the laser excitation power at the uniaxial strains of 0 % and 1.02 %. The black line and red line represent the power law fitting corresponding to each excitation wavelength. (For interpretation of the references to colour in this figure legend, the reader is referred to the Web version of this article.)

$x$ is around 0.5 for the measured 1L-WSSe alloy flake. The peak position of PL emission in 1L-WSSe alloy is redshifted continuously when the uniaxial tensile strain changes gradually from 0 % to 1.02 %, and there is noticeable increase in the PL intensity. As plotted in Fig. 4(b), the UPL spectra acquired from the same 1L-WSSe flake under uniaxial strain up to 1.02 % shows the redshifted peak position of UPL emission and the greatly enhanced UPL intensity as the strain increases. Fig. 4(c) summarizes the linear relationship between the peak position and the applied uniaxial strain for the PL and UPL spectra shown in Fig. 4(a) and (b). It is observed that the peak position of PL emission is redshifted about 23.8 nm at 1.02 % uniaxial strain compared to 0 % strain, giving the linear slope of around 23.3 nm/% strain due to the reduced bandgap of 1L-WSSe alloy under strain. The UPL peak position is also redshifted about 25.6 nm as the strain goes up to 1.02 % compared to the peak position of 678.8 nm at 0 % strain, and the linear slope is around 25.1 nm/% strain which corresponds to a gauge factor in UPL strain tuning with a value of 65.1 meV/% strain. As the uniaxial tensile strain exerted on 1L-WSSe alloy increases from 0 % to 1.02 %, the upconversion energy difference calculated from the photon energy of excitation and the photon energy of UPL emission with $\Delta E = \hbar\omega_{ex.} - \hbar\omega_{UPL}$ varies from −197 meV to −131 meV under the excitation at 761 nm. Fig. 4(d) further plots the integrated UPL intensity depending on the applied uniaxial tensile strain, showing an exponential increase of the UPL intensity by 4.9 times when the strain is tuned. The integrated UPL intensity depends on the upconversion energy difference $\Delta E$, which follows the Boltzmann function of $I_{UPL} \propto exp(\Delta E/k_B T)$ with the Boltzmann constant $k_B$ and the room temperature $T$ of 298 K. The UPL process in 1L-TMDs is mediated by the multiphonon absorption of the out-of-plane $A_{1g}$ transverse optical

phonons, rather than the in-plane $E^1_{2g}$ longitudinal optical phonons, which is indicated by the preservation of valley polarization in consistence with the polarization properties of the $A_{1g}$ phonon, along with the symmetry of the electronic states within the K valleys [22,24]. Since the 1L-WSSe alloy supports three $A_{1g}$ transverse optical phonon modes with the Raman shifts at 258 $cm^{-1}$ ($A_{1g}$ (Se–W)), 384 $cm^{-1}$ ($A_{1g}$ (S–W–Se)), and 404 $cm^{-1}$ ($A_{1g}$ (S–W)) that correspond to the phonon energy of approximately 32 meV, 48 meV, and 50 meV, respectively, the average number of phonons involved in the multiphonon-mediated upconversion process in 1L-WSSe alloy is approximately estimated as 6 to 4, 4 to 2, and 4 to 2 for each $A_{1g}$ transverse optical phonon as the uniaxial tensile strain is applied, according to the ratio between $|\Delta E|$ and the phonon energy. It is noted that the average number of phonons is used here to characterize the statistical distribution of multiphonon interactions involved in the UPL process, which bridges the upconversion energy difference $\Delta E$ between the excitation photon energy and the emission photon energy. It is expected that the coupling strengths between phonons and excitons will vary for each phonon mode with different phonon energy and vibrational properties. As the exerted uniaxial tensile strain increases, the average number of phonons associated with the UPL emission process in 1L-WSSe alloy is reduced. The UPL emission energy $\hbar\omega_{UPL}$ decreases almost linearly with the exerted uniaxial tensile strain $\varepsilon$, with $\hbar\omega_{UPL}(\varepsilon) \approx \hbar\omega_{UPL}(0\ \%) - g\varepsilon$ where $g$ is the gauge factor in UPL strain tuning, so that the UPL intensity in 1L-WSSe alloy as a function of the applied uniaxial tensile strain can be expressed as $I_{UPL} \propto exp(g\varepsilon/k_BT)$. As shown in Fig. 4(d), the measured integrated UPL intensity in 1L-WSSe alloy is well fitted by this exponential expression.

Fig. 5(a)–(d) present the power dependence plots of PL and UPL spectra under 532 nm and 761 nm excitations with the applied uniaxial strains of 0 % and 1.02 % on 1L-WSSe alloy. It shows that the spectral shapes and peak positions of PL and UPL spectra are well maintained for all the excitation powers, while the PL intensity and UPL intensity rise gradually as the laser excitation power is increased. Fig. 5(e) and (f) display the power dependent integrated PL and UPL intensities under the excitation at 532 nm and 761 nm in log-log scale at the applied uniaxial strains of 0 % and 1.02 %. The power law $I = \alpha P^{\beta}$ between the emission intensity $I$ and the excitation power $P$ is utilized to fit the measured integrated PL intensity and UPL intensity, with the fitting parameter $\alpha$ and the exponent $\beta$. The fitted $\beta$ values for the PL emission under both uniaxial tensile strains of 0 % and 1.02 % indicate the sublinear power dependence of PL emission, which is caused by the strong PL response of 1L-WSSe alloy and the saturated absorption at low excitation power in μW level. At the same time, the fitted $\beta$ values for the UPL emission under both uniaxial strains also suggest a sublinear power dependence, which can be associated with the variation of densities of phonons and exciton complexes [24]. The obtained sublinear power dependence for UPL emission in 1L-WSSe alloy under uniaxial tensile strain shows the multiphonon-mediated upconversion emission process involved with one photon, which is different from optical nonlinear processes including two-photon absorption process and Auger recombination process.

## 4. Conclusion

The UPL emission in 1L-WSSe alloy flakes on flexible substrate under uniaxial tensile strain at room temperature has been demonstrated. When the uniaxial tensile strain exerted on 1L-WSSe alloy changes from 0 % to 1.02 %, the peak position of UPL emission excited at the wavelength of 761 nm is redshifted by around 25.6 nm which corresponds to a gauge factor in UPL strain tuning with a value of 65.1 meV/% strain. The UPL intensity in 1L-WSSe alloy increases exponentially depending on the applied uniaxial tensile strain with the enhancement of 4.9 times as the upconversion energy difference varies from −197 meV to −131 meV. The sublinear power dependence for UPL emission in 1L-WSSe alloy with uniaxial strain shows the clear evidence of the multiphonon-mediated upconversion emission process involved with one photon. The demonstrated strain-tunable UPL emission in 1L-TMD alloy platforms with both compositional tunability and mechanically tuned emission properties will hold promises for integrating upconversion-based functionalities into future strain-programmable flexible or wearable photonic and optoelectronic devices such as strain sensors, tunable quantum light sources, and bioimaging platforms that operate under low-energy excitation conditions.

## CRediT authorship contribution statement

**Shrawan Roy:** Writing – original draft, Formal analysis. **Jie Gao:** Writing – review & editing, Investigation, Conceptualization. **Xiaodong Yang:** Writing – review & editing, Investigation, Conceptualization.

## Declaration of competing interest

The authors declare that they have no known competing financial interests or personal relationships that could have appeared to influence the work reported in this paper.

## Acknowledgments

The authors acknowledge the support from the DARPA (W911NF2110353). The authors also thank Brian Porter and Md. Kazi Rokunuzzaman for their help in acquiring the XPS data.

## Data availability

Data will be made available on request.

## References

[1] S. Roy, W. Choi, S. Jeon, D.-H. Kim, H. Kim, S.J. Yun, Y. Lee, J. Lee, Y.-M. Kim, J. Kim, Atomic observation of filling vacancies in monolayer transition metal sulfides by chemically sourced sulfur atoms, Nano Lett. 18 (7) (2018) 4523–4530.
[2] K.P. Dhakal, S. Roy, S.J. Yun, G. Ghimire, C. Seo, J. Kim, Heterogeneous modulation of exciton emission in triangular $WS_2$ monolayers by chemical treatment, J. Mater. Chem. C 5 (2017) 6820–6827.
[3] S. Roy, G.P. Neupane, K.P. Dhakal, J. Lee, S.J. Yun, G.H. Han, J. Kim, Observation of charge transfer in heterostructures composed of $MoSe_2$ quantum dots and a monolayer of $MoS_2$ or $WSe_2$, J. Phys. Chem. C 121 (3) (2017) 1997–2001.
[4] S. Roy, M.-H. Doan, J. Kim, S.K. Kang, G.H. Ahn, H.S. Lee, S.J. Yun, J. Kim, Modulation of optoelectric properties of monolayer transition metal dichalcogenides placed on a metal pattern, J. Kor. Phys. Soc. 78 (2021) 693–699.
[5] S. Tongay, D.S. Narang, J. Kang, W. Fan, C.H. Ko, A.V. Luce, K.X. Wang, J. Suh, K. D. Patel, V.M. Pathak, J.B. Li, J.Q. Wu, Two-dimensional semiconductor alloys: monolayer $Mo_{1-x}W_xSe_2$, Appl. Phys. Lett. 104 (2014) 012101.
[6] Y.F. Chen, J.Y. Xi, D.O. Dumcenco, Z. Liu, K. Suenaga, D. Wang, Z.G. Shuai, Y. S. Huang, L.M. Xie, Tunable band gap photoluminescence from atomically thin transition-metal dichalcogenide alloys, ACS Nano 7 (5) (2013) 4610–4616.
[7] J. Park, M.S. Kim, B. Park, S.H. Oh, S. Roy, J. Kim, W. Choi, Composition-tunable synthesis of large-scale $Mo_{1-x}W_xS_2$ alloys with enhanced photoluminescence, ACS Nano 12 (6) (2018) 6301–6309.
[8] Q.L. Feng, N.N. Mao, J.X. Wu, H. Xu, C.M. Wang, J. Zhang, L.M. Xie, Growth of $MoS_{2(1-x)}$ $Se_{2x}$ ($x$ = 0.41–1.00) monolayer alloys with controlled morphology by physical vapor deposition, ACS Nano 9 (7) (2015) 7450–7455.
[9] X.D. Duan, C. Wang, Z. Fan, G.L. Hao, L.Z. Kou, U. Halim, H.L. Li, X.P. Wu, Y. C. Wang, J.H. Jiang, A.L. Pan, Y. Huang, R.Q. Yu, X.F. Duan, Synthesis of $WS_{2x}Se_{2-2x}$ alloy nanosheets with composition-tunable electronic properties, Nano Lett. 16 (1) (2016) 264–269.
[10] F.A. Nugera, P.K. Sahoo, Y. Xin, S. Ambardar, D.V. Voronine, U.J. Kim, H. Son, H. R. Gutiérrez, Bandgap engineering in 2D lateral heterostructures of transition metal dichalcogenides via controlled alloying, Small 18 (2022) 2106600.
[11] G. Bacher, C. Hartmann, H. Schweizer, T. Held, G. Mahler, H. Nickel, Exciton dynamics in InxGa1−xAs/GaAs quantum-well heterostructures: competition between capture and thermal emission, Phys. Rev. B 47 (15) (1993) 9545.
[12] Z. Deutsch, L. Neeman, D. Oron, Luminescence upconversion in colloidal double quantum dots, Nat. Nanotechnol. 8 (9) (2013) 649.
[13] F. Auzel, Upconversion and anti-stokes processes with f and d ions in solids, Chem. Rev. 104 (1) (2004) 139.
[14] S. Baluschev, T. Miteva, V. Yakutkin, G. Nelles, A. Yasuda, G. Wegner, Up-conversion fluorescence: noncoherent excitation by sunlight, Phys. Rev. Lett. 97 (14) (2006) 143903.
[15] J. Zhao, S. Ji, H. Guo, Triplet–triplet annihilation based upconversion: from triplet sensitizers and triplet acceptors to upconversion quantum yields, RSC Adv. 1 (6) (2011) 937–950.

[16] Z. Feng, T. Shi, G. Geng, J. Li, Z.-L. Deng, Y. Kivshar, X. Li, Dual-band polarized upconversion photoluminescence enhanced by resonant dielectric metasurfaces, eLight 3 (2023) 21.
[17] S. Roy, X. Yang, J. Gao, Uniaxial strain tuning upconversion photoluminescence in monolayer $WSe_2$, Adv. Photonics Res. 5 (2024) 2300220.
[18] S. Roy, J. Gao, X. Yang, Upconversion photoluminescence of monolayer $WSe_2$ with biaxial strain tuning, Opt. Express 32 (3) (2024) 3308–3315.
[19] S. Roy, X. Yang, J. Gao, Biaxial strain tuned upconversion photoluminescence of monolayer $WS_2$, Sci. Rep. 14 (2024) 3860.
[20] F. Meng, X. Yang, J. Gao, High-temperature phonon-assisted upconversion photoluminescence of monolayer $WSe_2$ at elevated temperature, Appl. Phys. Lett. 123 (2023) 013502.
[21] F. Meng, X. Yang, J. Gao, Phonon-assisted upconversion photoluminescence of monolayer $MoS_2$ at elevated temperature, Opt. Express 31 (2023) 28437–28443.
[22] A.M. Jones, H. Yu, J.R. Schaibley, J. Yan, D.G. Mandrus, T. Taniguchi, K. Wantabe, H. Dery, W. Yao, X. Xu, Excitonic luminescence upconversion in a two-dimensional semiconductor, Nat. Phys. 12 (2016) 323–327.
[23] M. Manca, M.M. Glazov, C. Robert, F. Cadiz, T. Taniguchi, K. Wantabe, E. Courtade, T. Amand, P. Renucci, X. Marie, G. Wang, B. Urbaszek, Enabling valley selective exciton scattering in monolayer $WSe_2$ through upconversion, Nat. Commun. 8 (2017) 14927.
[24] J. Jadczak, L. Bryja, J. Kutrowska-Girzycka, P. Kapuściński, M. Bieniek, Y.-S. Huang, P. Hawrylak, Room temperature multi-phonon upconversion photoluminescence in monolayer semiconductor $WS_2$, Nat. Commun. 10 (2019) 107.
[25] A. Mushtaq, X. Yang, J. Gao, Unveiling room temperature upconversion photoluminescence in monolayer $WSe_2$, Opt. Express 30 (25) (2022) 45212–45220.
[26] E. Downing, L. Hesselink, J. Ralston, R. Macfarlane, A three-color, solid-state, three-dimensional display, Science 273 (5279) (1996) 1185–1189.
[27] V. Gray, D. Dzebo, M. Abrahamsson, B. Albinsson, K. Moth-Poulsen, Triplet–triplet annihilation photon-upconversion: towards solar energy applications, Phys. Chem. Chem. Phys. 16 (22) (2014) 10345–10352.
[28] C.T. Xu, N. Svensson, J. Axelsson, P. Svenmarker, G. Somesfalean, G. Chen, H. Liang, H. Liu, Z. Zhang, S. Andersson-Engels, Autofluorescence insensitive imaging using upconverting nanocrystals in scattering media, Appl. Phys. Lett. 93 (17) (2008) 171103.
[29] C. Vinegoni, D. Razansky, S.A. Hilderbrand, F. Shao, V. Ntziachristos, R. Weissleder, Transillumination fluorescence imaging in mice using biocompatible upconverting nanoparticles, Opt. Lett. 34 (17) (2009) 2566–2568.
[30] G.S. He, P.P. Markowicz, T.-C. Lin, P.N. Prasad, Observation of stimulated emission by direct three-photon excitation, Nature 415 (6873) (2002) 767–770.
[31] R.I. Epstein, M.I. Buchwald, B.C. Edwards, T.R. Gosnell, C.E. Mungan, Observation of laser-induced fluorescent cooling of a solid, Nature 377 (6549) (1995) 500–503.
[32] R. Roldán, A. Castellanos-Gomez, E. Cappelluti, F. Guinea, Strain engineering in semiconducting two-dimensional crystals, J. Phys. Condens. Matter 27 (2015) 313201.
[33] S.B. Desai, G. Seol, J.S. Kang, H. Fang, C. Battaglia, R. Kapadia, J. W Ager, J. Guo, A. Javey, Strain-induced indirect to direct bandgap transition in multilayer $WSe_2$, Nano Lett. 14 (8) (2014) 4592–4597.
[34] W. Wu, J. Wang, P. Ercius, N.C. Wright, D.M. Leppert-Simenauer, R.A. Burke, M. Dubey, A.M. Dogare, M.T. Pettes, Giant mechano-optoelectronic effect in an atomically thin semiconductor, Nano Lett. 18 (4) (2018) 2351–2357.
[35] J.O. Island, A. Kuc, E.H. Diependaal, R. Bratschitsch, H.S.J. Van der Zant, T. Hiene, A. Castellanos-Gomez, Precise and reversible band gap tuning in single-layer $MoSe_2$ by uniaxial strain, Nanoscale 8 (2016) 2589–2593.
[36] F. Carrascoso, H. Li, R. Frisenda, A. Castellanos-Gomez, Strain engineering in single-, bi- and tri-layer $MoS_2$, $MoSe_2$, $WS_2$ and $WSe_2$, Nano Res. 14 (6) (2021) 1698–1703.
[37] F. Carrascoso, R. Frisenda, A. Castellanos-Gomez, Biaxial versus uniaxial strain tuning of single-layer $MoS_2$, Nano Mater. Sci. 4 (1) (2022) 44–51.
[38] K.P. Dhakal, S. Roy, H. Jang, X. Chen, W.S. Yun, H. Kim, J.D. Lee, J. Kim, J.-H. Ahn, Local strain induced band gap modulation and photoluminescence enhancement of multilayer transition metal dichalcogenides, Chem. Mater. 29 (12) (2017) 5124–5133.
[39] H. Li, A.W. Contryman, X. Qian, S.M. Ardakani, Y. Gong, X. Wang, J.M. Weisse, C. H. Lee, J. Zhao, P.M. Ajayan, H.C. Manoharan, X. Zheng, Optoelectronic crystal of artificial atoms in strain-textured molybdenum disulphide, Nat. Commun. 6 (2015) 7381.
[40] J. Chaste, A. Missaoui, S. Huang, H. Henck, Z.B. Aziza, L. Ferlazzo, C. Naylor, A. Balan, A.T. C. J Jr., R. Braive, A. Ouerghi, Intrinsic properties of suspended $MoS_2$ on $SiO_2$/Si pillar arrays for nanomechanics and optics, ACS Nano 12 (4) (2018) 3235–3242.
[41] J. Wang, M. Han, Q. Wang, Y. Ji, X. Zhang, R. Shi, Z. Wu, L. Zhang, A. Amini, L. Guo, N. Wang, J. Lin, C. Cheng, Strained epitaxy of monolayer transition metal dichalcogenides for wrinkle arrays, ACS Nano 15 (4) (2021) 6633–6644.
[42] Q. Zhao, T. Wang, Y.K. Ryu, R. Frisenda, A.J. Castellanos-Gomez, An inexpensive system for the deterministic transfer of 2D materials, Phys. Mater. 3 (2020) 016001.